Electrochemical Behavior of Three 90Cu-10Ni Tubes from Different Manufacturers After Immersion in 3.5% NaCl Solution

Okpo O. Ekerenam, Aili Ma, Yugui Zheng, and Wilfred Emori

Investigation on the electrochemical behavior and corrosion product films formed on three 90Cu-10Ni tubes designated as Tubes A, B and C from three different manufacturers with different service lives were carried out using electrochemical techniques, SEM, XRD and XPS after immersion in 3.5 wt.% NaCl solution. The results of polarization curve measurements showed noticeable decrease in the corrosion current densities (I_{corr}) of the three tubes with immersion time, and the I_{corr} of Tube C was comparatively lower than those of Tubes A and B at early immersion period. EIS measurements revealed duplex film layers on the surface of the samples with the inner film formation occurring at different times for different tubes as the film resistance R_{f2} revealed the formation of the inner compact layer in Tube C after 15-day immersion and in Tubes A and B after 30 days. Tube C showed better corrosion resistance which is due to early formation of the inner compact oxide film. The XPS analysis revealed Ni enrichment on the surface film of the three samples but Ni depletion as the immersion time is increased.

1. Introduction

Cu-Ni alloys are considered very important commercial alloys in the marine environment. The 90Cu-10Ni alloy has shown good corrosion resistance in seawater, so it has found a wide use in different marine industries such as the heat exchanger tubes in ships (Ref 1). It has been reported that copper-nickel alloys form a homogeneous, α-solid solution over the complete range of Cu-Ni composition (Ref 2). Alloying elements such as nickel and iron are generally accepted to improve corrosion resistance through modification of aged surface oxide layers (Ref 3, 4). The good resistance of the alloy to seawater corrosion is generally attributed to the formation of a protective oxide film on the alloy surface when exposed to seawater (Ref 5-10). This protective oxide film is a duplex layer comprising of an outer layer of cupric hydroxyl chloride, $Cu_2(OH)_3Cl$, overlaying a compact inner layer of cuprous oxide, Cu_2O, with nickel and iron incorporated occupying cation vacancies and thus increasing the corrosion resistance (Ref 11). However, despite its resistance to seawater corrosion, premature failures of the 90Cu-10Ni alloy tubes are reported frequently after several months of exposure (Ref 12, 13). These failures may be due to (1) external conditions, including water contamination, e.g., hydrogen sulfide ion (Ref 14), higher flow velocity, and/or

disturbed flows (Ref 15), and (2) material factors, such as alloy element segregation, microstructure inhomogeneity, impurities and the grain boundary defects (Ref 16, 17).

Despite having similar compositions and applied in identical conditions, product users report that there exist differences in the service life of 90Cu-10Ni alloy tubes delivered by different manufacturers. There is, however, no clear explanation as to the reasons behind these disparities in service life of the 90Cu-10Ni alloy tubes. Ma et al. (Ref 18) correlated between microstructure and corrosion behavior of two 90Cu-10Ni tubes with significantly different service lives. They concluded that a special "grain boundary engineering" (GBE) treatment must have been performed on the tube with longer service life. However, there is no systematic study on the corrosion behavior of these alloy tubes delivered by different manufacturers using electrochemical techniques. It is therefore necessary to carry out a comparative work on the electrochemical behavior of 90Cu-10Ni alloy tubes delivered by different manufacturers to understand their different corrosion resistance in service environment.

This work investigated the corrosion behavior of three 90Cu-10Ni alloy tubes delivered by different manufacturers in 3.5% NaCl solution using electrochemical measurements such as open-circuit potential (OCP), linear polarization resistance, potentiodynamic polarization curves, electrochemical impedance spectroscopy (EIS), and the corresponding corrosion product film using SEM, XRD and XPS, with the aim to understand the differences in corrosion behavior of the tubes. The main focus is on the dependence of the corrosion resistance of surface oxide film on immersion time.

2. Experimental

2.1 Materials and Metallography

The experimental materials are three 90Cu-10Ni alloy tubes, supplied by three domestic or oversea manufacturers and

Okpo O. Ekerenam, Aili Ma, Yugui Zheng, and **Wilfred Emori,** CAS Key Laboratory of Nuclear Materials and Safety Assessment, Institute of Metal Research, Chinese Academy of Sciences, 62 Wencui Road, Shenyang 110016, People's Republic of China. Contact e-mail: alma@imr.ac.cn.

denoted as Tube A (service life ≈1 year), Tube B (service life ≈3 years) and Tube C (service life is unknown), respectively. The chemical compositions of the tubes are shown in Table 1. The specimens for metallography observation were cut from the cross section of the tubes, sealed with the Bakelite resin, and then ground with a series of SiC abrasive papers (grit size 400, 600, 800, 1500 and 2000), followed by polishing with a 1.0-μm diamond paste and etching with an etchant of 5 g ferric chloride +2 ml hydrochloric acid +96 ml ethanol.

The EBSD experiment was performed on cross sections of the three tubes to obtain their grain size distribution. Prior to the experiment, the samples were prepared by firstly sealing with the room temperature-curing denture base resin, then grinding mildly using 1000, 2000, 3000 and 5000 grid silicon carbide papers, and finally electropolishing in a solution of phosphoric acid:ethanol:water = 1:1:2 (in volume fraction) at a DC voltage of 28 V for ≈90 s. The samples were put into the SEM chamber for EBSD scanning after the sealing resin was removed.

The EBSD experiment was conducted using the TSL laboratories orientation imaging microscopy (OIM) system attached to a JSM-6301 field emission gun SEM. The scanning step was set as 1 μm. The number of scanned points is 263,836 for the three samples. Two neighboring scan points were supposed to belong to the same grain if the misorientation between them was <5°. The minimum grain size allowable during statistics processing was set as two points (2 μm). The grain size distributions of Tubes A, B and C were obtained by the OIM ANALYSIS 5.2 software.

2.2 Immersion Test in 3.5 wt.% NaCl Solution

Tube A and Tube B were cut into pieces of 1 cm × 1 cm, and Tube C was cut into size of 1 cm × 0.5 cm due to its smaller diameter. The inner walls of the specimens were ground flat with SiC abrasive papers. Resin was prepared and the samples embedded in it through the help of plastic tubes after being welded with wire. The embedded samples were left inside the drier for 12 h at the temperature of 45 °C to solidify and were then polished with 150, 400, 800, 1000 grits of SiC abrasive papers, washed with water, rinsed with ethanol and dried with hot air ready for use.

Immersion test in the laboratory was carried out in 3.5 wt.% NaCl solution to investigate their different corrosion behavior. A 3.5 wt.% NaCl solution was prepared by analytical grade NaCl and distilled water to simulate seawater for the immersion test.

Open-circuit potential (OCP), linear polarization resistance (LPR), electrochemical impedance spectra (EIS) and potentiodynamic polarization curves were tested after 0-, 1-, 3-, 7-, 15-, 30-, 45-, 60-, 75-, 90-day immersion for the samples of Tubes A, B and C. The measurements were taken using an experimental setup which consists of Gamry Reference 1000 potentiostat/galvanostat/ZRA system and three electrode systems with platinum electrode as the counter electrode. Saturated calomel electrode (SCE) was used as the reference electrode and the sample as the working electrode.

The open-circuit potential measurements were taken for 3600 s. Linear polarization sweeping was executed from −10 to +10 mV (versus OCP) with a scan rate of 0.125 mV s^{-1}. EIS measurements were taken over the frequency range of 100 kHz to 10 mHz with AC potential signal of 10 mV at the open-circuit potential. Potentiodynamic scan was carried out at the voltage range of −500 and +1200 mV (versus OCP) with the scan rate of 0.5 mV s^{-1}. All the measurements were repeated at least three times to ensure good reproducibility. The obtained data were analyzed using Gamry Echem Analyst (version 6.11) software.

2.3 Corrosion Product Film Characterization

2.3.1 Morphology Analysis by SEM. To characterize the corrosion product film, the cross-sectional morphology and surface morphology of the three samples were observed by a scanning electron microscope (SEM) (FEI, INSPECT F50) after 15- and 30-day immersion periods. While the samples for surface morphology were detected directly after being retrieved from 3.5 wt.% NaCl solution, samples for cross-sectional morphology were mounted with the Bakelite resin and then slowly ground down to 3000 grit SiC paper and mildly polished with 1.0-μm diamond paste. Before being put into the SEM chamber, both the surface and the cross-sectional samples were sprayed with a carbon coat on its surface in order to enhance the conductivity of the corrosion product film. The imaging sites for SEM were randomly chosen on the specimen surface to be representative of the entire surface of the alloy specimens.

2.3.2 XRD Analysis. The phase components of the corrosion product films were analyzed by x-ray diffraction (Pananalytical X' Pert PRO, Cu Ka radiation at 40 kV, PA Analytical, Almelo, Holland) with a 2.0° min^{-1} scanning speed and a 10°-90° of 2θ range. The samples were detected as retrieved from the solution after 15- and 30-day immersion periods.

2.3.3 XPS Analysis. To further understand the evolution of the surface films with exposure time on the three tubes and the nature of their composition at various depths within the corrosion product film, detailed XPS study was conducted after 15- and 30-day immersion in 3.5 wt.% NaCl solution. The films of approximately 2 μm were too thick to be sputtered through by argon ions so as to collect signals of elements at different layers within the film. Therefore, a method of scrapping and sputtering was applied. To be specific, after being retrieved from 3.5 wt.% NaCl solution, the corrosion product film on the samples of 1 cm × 1 cm for Samples A and B and 1 cm × 0.5 cm for Sample C were scrapped off slightly by the surface of a cylinder rolled from a fine abrasive paper till the alloy substrate was exposed. Then, the samples were put into the XPS chamber, and the signals of the outer layer of the film were collected after sputtering for 0, 20, 60, 140, 300, 620 and 1260 s at the original surface of the film and the signals of

Table 1 Chemical composition (wt.%) of the three experimental 90Cu-10Ni alloy tubes

Material	Ni	Fe	Mn	C	Pb	S	P	Zn	Cu
Tube A	10.4	1.73	0.68	0.014-0.027	<0.001	0.004	0.003	<0.01	Bal.
Tube B	10.4	1.51	0.59	0.009	<0.001	0.002	0.002	<0.01	Bal.
Tube C	9.81	1.17	0.64	0.006	<0.0005	0.0026	0.003	0.005	Bal.

the inner layer collected after sputtering for 0, 20, 60, 140 and 300 s at the slope between the exposed alloy substrate and the original surface formed by the scrapping process mentioned above.

The XPS measurement was taken using a VG ESCALAB 250 x-ray photoelectron spectrometer. The photoelectrons were excited with Al Ka (1486.6 eV) x-ray source, and the analyzer pass energy was 50.0 eV. Binding energies (BEs) were calibrated against the surface carbon contamination at 284.6 eV. Composition depth profiles were obtained with 2.0 keV argon ions at a target current of 2.0 µA cm^{-2} and a pressure of 7.7×10^{-9} MPa. The sputtering rate was estimated to be about 0.2 nm s^{-1} (versus Ta_2O_5). The XPS PEAK software, based on a nonlinear least-square regression method, was used to implement the fitting process.

3. Results and Discussion

3.1 Chemical Composition and Metallographic Examination

From Table 1, all the elemental components of the tubes were within American Standard of Testing Materials (ASTM) quoted by Schleich (Ref 19) for 90Cu-10Ni alloy used as tubing materials. Thus, the corrosion behavior of these tubes is not related to the use of substandard materials. The addition of iron is known to increase the resistance to impingement attack by flowing seawater (Ref 20).

The optical micrographs comparing the cross-sectional metallographic structures of Tubes A, B and C are presented in Fig. 1(a), (b), and (c). The grains are equiaxed, and there are many annealing twins with straight band morphology in the three tubes, which is a typical microstructure of an annealed low stacking fault energy alloy. Their grain size distributions are displayed in Fig. 1(d), (e) and (f). The average grain sizes for Tubes A, B and C are 36.4, 33.6 and 21.1 µm, respectively, and the standard deviations of their grain sizes are 13.2, 12.5 and 7.0 µm, respectively. In addition, it seems that more residual strain exists in the structure of Tube C compared with Tube A and Tube B.

3.2 Open-Circuit Potential Measurements

The OCPs for the three tubes after immersion in 3.5 wt.% NaCl are presented in Fig. 2 for Samples A, B and C, respectively. The values generally decreased until certain immersion time before becoming more positive at longer immersion periods. The negative shift in the OCPs of the three samples indicates a dissolution process of the metal in the electrolyte before the formation of a protective oxide film. After longer immersion, the OCPs shifted to more positive values depicting the formation of a protective layer which reduces the corrosion rate.

The OCPs of the three samples showed similar behavior except different transition time from active to passive behavior which is shown after 30, 30 and 45 days for Samples A, B and C, respectively.

3.3 Linear Polarization Resistance

Figure 3 shows the dependence of linear polarization resistance (R_p) of Samples A, B and C on immersion time. Triplicate analyses were carried out to ensure the result's reproducibility. The R_p of the three samples increased with immersion time at the early stage of immersion and then remained fairly unchanged after 15 days for Samples A and B and 30 days for Sample C. It is worthy of note that Samples A and B showed similar behavior, while Sample C gives higher R_p values after 30 days which may result in a better resistance to corrosion.

## 3.4 Potentiodynamic Polarization Measurements

Figure 4(a), (b), and (c) presents potentiodynamic polarization curves of the samples after varied exposure times. The fitted data are presented in Tables 2, 3, and 4 for Samples A, B and C, respectively. It can be observed that the anodic portion of the potentiodynamic curves showed similar behavior with little differences in the corrosion current densities for the samples studied. Therefore, the cathodic portions were fitted using Gamry software to obtain corrosion current density (I_{corr}), corrosion potential (E_{corr}) and Tafel slope. I_{corr} decreased with increase in the immersion time for the three samples and dramatically reduced from initially 4.47 to 0.27, 4.13 to 0.5 and 2.17 to 0.59 µA cm^{-2} after 90-day immersion time for Samples A, B and C, respectively, indicating a decrease in the corrosion rate of the tubes due to the formation of the protective oxide film layer (Ref 21, 22). Also, the I_{corr} rapidly decreased for the three samples with time at the early immersion period (between 0 and 3 days) but became more stable with little changes until after 90-day immersion period. This can be attributed to the compactness of the protective film as the immersion time is increased and this prevents the metal surface from further attack by the chloride ions in the electrolyte solution. This is in agreement with Druska et al. (Ref 11) which reported that the protective oxide film on the surface of Cu-Ni alloys immersed in seawater becomes more compact as the immersion time is increased.

Corrosion potential E_{corr} showed fluctuations between -276.5 and -356.8, -309.4 and -514.2, and -276.8 and -406.8 mV for Samples A, B and C, respectively, throughout the immersion test. The shift in E_{corr} to negative or positive potential is due to changes in the film formed on the surface of the metal alloy as the corrosion behavior depends strongly on the nature of the barrier film (Ref 23).

3.5 Electrochemical Impedance Measurements

The electrochemical impedance spectra of the samples in simulated seawater after different immersion times are shown in Fig. 5, 6, and 7 (a, b and c for Samples A, B and C, respectively). Tables 5, 6, and 7 present the corresponding fitted data of the EIS results.

Kinetics of the electrochemical process can be identified and quantified form the low-frequency impedance. Bode plots (Fig. 5a-c) showed that the total impedance magnitudes of the samples at the lower frequency range increased with immersion time, indicating that the corrosion resistance increased with time as the oxide film was formed (Ref 24-27). It later decreased at longer immersion period for Samples A and C which may be as the result of film breakdown. In contrast, Sample B impedance increased initially before fluctuating with time but displayed its highest impedance after 90 days suggesting good resistance to corrosion at longer immersion time. From the respective phase angle bode plots (Fig. 6a-c), for some immersion periods only one broad peak maximum
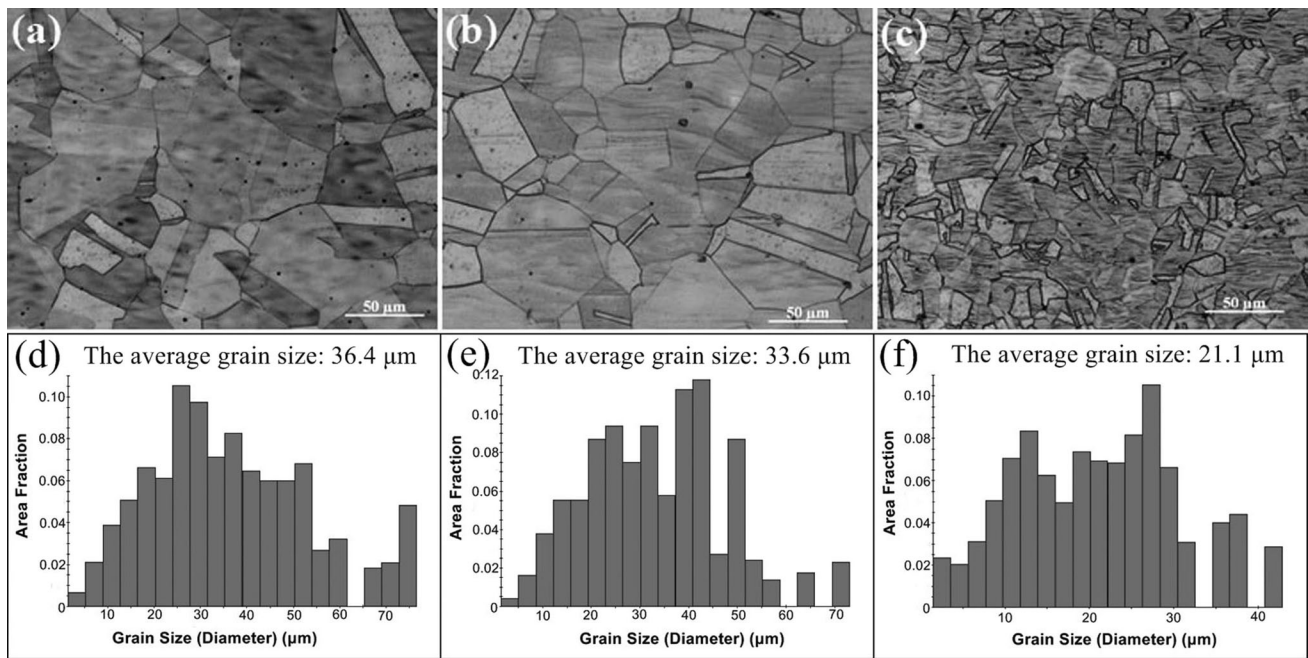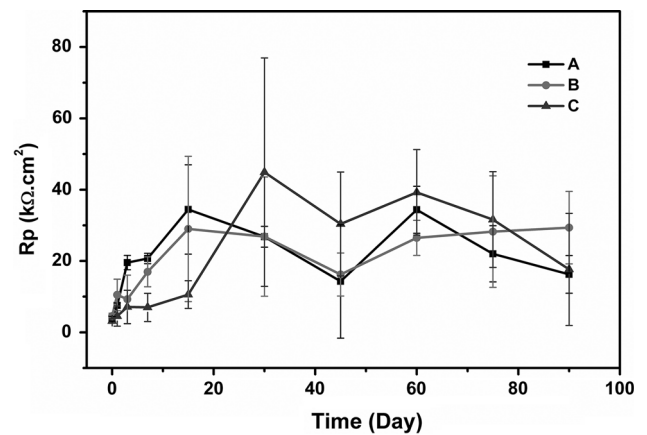
Fig. 1 Optical micrographs (a, b and c) on cross sections of Tubes A, B and C, respectively, and their grain size distributions (d, e and f) corresponding to Tubes A, B and C, respectively
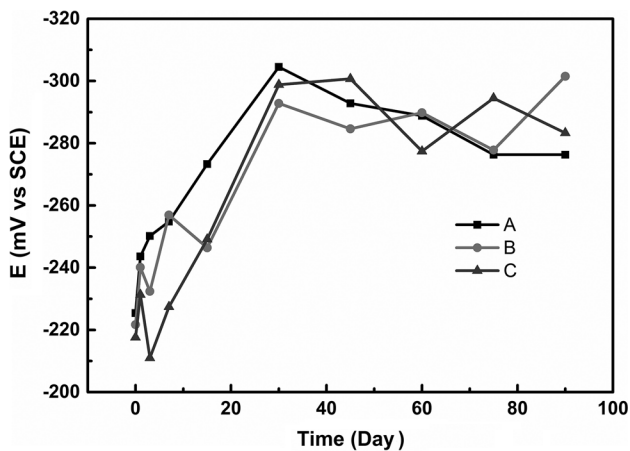
Fig. 2 OCP measurements for Samples A, B and C after 0-, 1-, 3-, 7-, 15-, 30-, 45-, 60-, 75-, 90-day immersion in 3.5% NaCl solution

Fig. 3 Comparison of the linear polarization resistance for Samples A, B and C after 0-, 1-, 3-, 7-, 15-, 30-, 45-, 60-, 75-, 90-day immersion in 3.5% NaCl solution

is distinguished for the three samples, suggesting two time constants with their characteristic frequencies close to each other, while for other immersion times two separated phase angle maxima can be identified apparently. The maximum peak angles all appeared at the low frequency range which may be derived from electrical double layer (EDL) and increased from about 60° to 73°, 60° to 76° and 58° to 68° for Samples A, B and C, respectively, with increase in immersion time from 0 to 90 days. The gradual increase in the phase maxima recorded with immersion time is caused by the increasing resistance of oxide film which in turn led to a decrease in the corrosion rate (Ref 10, 21, 25, 27, 28).

In the Nyquist plots as shown in Fig. 7(a), (b) and (c), the diameter of the impedance arcs initially increased with time, implying a decrease in the corrosion rate for the three samples.

The maximum arcs were attained at different times for the three samples (45, 15 and 30 days for sample A, B and C, respectively) which are the results of changes in the structures of the oxide films.

Impedance spectra of the samples were fitted using two different equivalent circuits as shown in Fig. 8 with the contribution of some phenomena [such as the electric double layer (EDL) and film(s) formation] being accounted for. Circuit 1 models two time constants and it is frequently used to represent the formation of a layer of oxide film on the metal surface, while Circuit 2 contains three time constants and it is used to show the formation of a duplex layer of surface film on the samples. Constant phase elements (CPEs) were introduced into the circuit to represent capacitance to avoid non-ideal behavior which may result from an inhomogeneous surface. The impedance of CPE, Q, can be expressed as
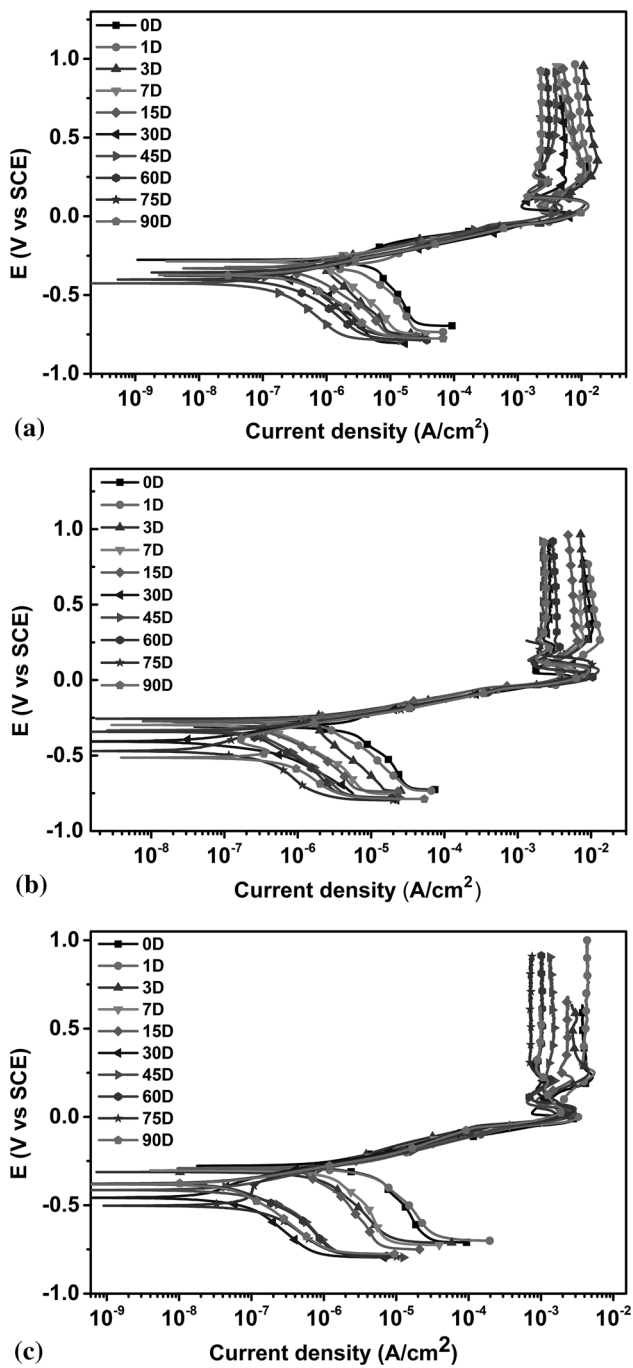
Fig. 4 Potentiodynamic polarization curves for Samples A, B and C after 0-, 1-, 3-, 7-, 15-, 30-, 45-, 60-, 75-, 90-day immersion in 3.5% NaCl solution

$Z_{CPE} = 1/[Y_0(j\omega)^n]$, where j is an imaginary number, $j = (-1)^{1/2}$, while ω $(=2\pi f)$ is the angular frequency (Ref 29). The power exponent n is an adjustable parameter that lies between 0 and 1 and can be used as the measure of the surface inhomogeneity (Ref 30). The factor Y denotes a parameter related to capacitance. Other circuit parameters are the resistances R_s, R_{ct}, R_{f1} and R_{f2} and can be defined as the solution resistance, the charge transfer resistance, the resistance of the outer film and the resistance of the inner film, respectively. The impedance spectra were fitted using equivalent Circuit 1 which models two relaxation time constants, from 0 to 15 days for

Samples A and B, and from 0 to 7 days for Sample C, while Circuit 2 which models three time constants was used to fit Samples A and B from 30 to 90 days and Sample C from 15 to 90 days, respectively. The fitted parameters of electrical components are listed in Tables 5, 6, and 7 for Samples A, B and C, respectively. The qualities of fitting are judged by Chi-square, χ^2, and are all $< 10^{-3}$, exhibiting the goodness of the fit. The combined effect of all the resistances or resultant resistance, R_{Total}, was calculated by taking the sum of individual resistance in series using the formula

$$R_{Total} = R_{ct} + R_{f1} + R_{f2}. \quad (Eq\ 1)$$

3.5.1 Film Formation at the Early Immersion Stage. It can be observed from Tables 5 and 6 that the film resistance, R_{f1}, markedly increased from 0 to 15 days for Samples A and B, while that of Sample C increased from 0 to 1 day and then gradually decreased but still maintained considerably high resistance as shown in Table 7. The reciprocal polarization resistance, R_p^{-1}, is proportional to the corrosion rate of the alloy through the Stern-Geary equation. And R_p here can be represented by the sum of R_{ct} and R_{f1}. The film resistance, R_{f1}, is much higher than the charge transfer resistance, R_{ct}, which means that the corrosion resistance of the samples during this period was determined by the film resistance and not the charge transfer resistance, so that increase in the film resistance implies a decrease in the corrosion rate of the alloy samples.

3.5.2 Film Formation at the Later Immersion Stage. It can be observed that at the later stages of immersion the film structure changed, leading to the formation of a duplex layer consisting of an outer porous layer and an inner compact layer as revealed by the resistances R_{f1} and R_{f2} for the three samples. After 30-day immersion time, the inner compact film was formed for Samples A and B, and its resistance increased until 60 days before it gradually decreased with time until 90 days as presented in Tables 5 and 6. Table 7 presents Sample C with similar behavior, but its inner film formation took place earlier (after 15 days) than Samples A and B. The n_3 values of Sample A were initially between 0.47 and 0.75 before increasing to 0.80, while that of Samples B and C showed increasing trend from 0.78 to 0.85 and 0.71 to 0.84, respectively. This indicates that the film gradually grew in thickness and compactness and it is in good agreement with previous report (Ref 14).

The resultant resistance from all the resistances, R_{Total}, calculated using Eq 1, showed that the resistance of Sample A increased continuously with time until after 60 days before decreasing gradually. Sample B showed similar behavior, but there is a drastic drop in the outer film resistance after 30 days leading to a corresponding decrease in R_{Total}, and R_{f1} then increased afterward with time until after 90 days. On the contrary, Sample C recorded high values of R_{Total} despite high fluctuations with time. It is also necessary to note that the inner film formation occurred at different time for the three samples as it took place after 30 days for Samples A and B and 15 days for Sample C, respectively. The Y values recorded were very low and showed decreasing trend as it fluctuated with time for the three samples, indicating the increase in compactness of the film with immersion time.

3.5.3 Dependence of Corrosion Resistance on Immersion Time. The corrosion resistance varies with immersion time for the three samples. This variation can be attributed to the changes in the film structure leading to active and passive

Table 2 Potentiodynamic polarization analysis data of Sample A after different immersion time in 3.5 wt.% NaCl solution

Time, days	Beta C, mV dec^{-1}	E_{corr}, mV	I_{corr}, μA cm^{-2}	Corr. rate, mpy
0	−498	−276.5	4.47	2.053
1	−298	−322.1	2.92	1.343
3	−337	−285.3	0.63	2.90E−01
7	−317	−286.4	0.81	3.70E−01
15	−259	−330.3	0.40	1.82E−01
30	−279	−376.6	0.38	1.72E−01
45	−270	−425.7	0.13	5.91E−02
60	−232	−401.8	0.19	8.64E−02
75	−328	−356.8	0.30	1.39E−01
90	−233	−372.9	0.27	1.25E−01

Table 3 Potentiodynamic polarization analysis data of Sample B after different immersion time in 3.5 wt.% NaCl solution

Time, days	Beta C, mV dec^{-1}	E_{corr}, mV	I_{corr}, μA cm^{-2}	Corr. rate, mpy
0	−352	−309.4	4.13	1.897
1	−244	−278.3	1.56	7.17E−01
3	−441	−256.4	1.25	5.72E−01
7	−257	−297.5	0.37	1.70E−01
15	−219	−272.9	0.20	9.27E−02
30	−226	−407.2	0.26	1.20E−01
45	−286	−333.1	0.26	1.19E−01
60	−257	−342.7	0.21	9.46E−02
75	−121	−363.4	0.32	1.46E−02
90	−263	−514.2	0.50	2.29E−01

Table 4 Potentiodynamic polarization analysis data of Sample C after different immersion time in 3.5 wt.% NaCl solution

| Time, days	Beta C, mV dec^{-1}	E_{corr}, mV	I_{corr}, μA cm^{-2}	Corr. rate, mpy
0	−524	−276.8	2.17	1.993
1	−351	−288.2	1.87	1.716
3	−353	−312.1	0.40	3.71E−01
7	−324	−303	0.50	4.55E−01
15	−276	−291	0.24	2.16E−01
30	−209	−405.3	0.27	2.44E−02
45	−280	−413.9	0.68	6.21E−02
60	−195	−377.6	0.25	2.33E−02
75	−171	−406.8	0.59	5.37E−02
90	−195	−435.6	0.31	2.88E−02

behavior. The increase in the film resistance (R_{f1}) at early immersion period is due to the presence of protective film on the surface of the samples which increased in thickness and compactness as the immersion time was increased. However, the film resistance gradually decreased at longer immersion periods due to continuous attack by chloride ions (Ref 31). It can be concluded that the outer film resistance decreased at longer immersion periods due to continuous contact with the electrolyte solution. At very early immersion periods (between 0 and 3 days), high resistance values were recorded for Sample C compared to Samples A and B. This may be the reason why its film resistance remained considerably high while decreasing as the immersion time is increased.

Formation of the inner barrier film (R_{f2}) consisting mainly of Cu$_2$O improves the resultant resistance, R_{Total}, of the samples to corrosion at the later time of immersion because of its

compactness as revealed in Tables 5, 6 and 7. It is also worthy of note that the formation of the inner barrier film took place at different time intervals. Early formation of the inner barrier film as well as its very high film resistances (up to 720 kΩ cm^2) at the early immersion period can be seen as the main reason Sample C showed better corrosion resistance compared to Samples A and B as shown in Fig. 9. This is in line with data from polarization curve measurements which reveal lower I_{corr} values for Sample C at the early immersion.

3.6 Cross-Section Morphology and Surface Analysis of the Corrosion Product Film
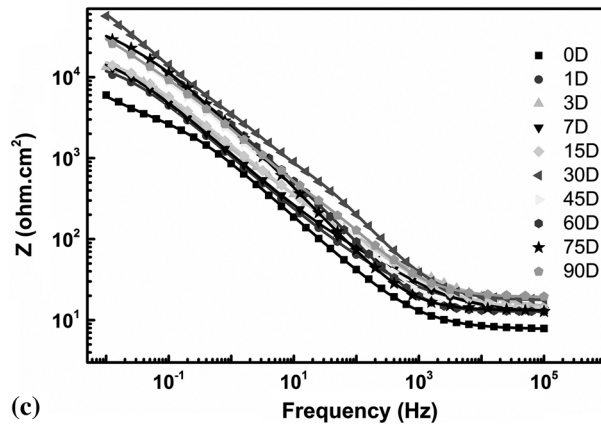
Figure 10(a), (b) and (c) and 11(a), (b) and (c) present the cross-section morphology after 15- and 30-day immersion for Samples A, B and C, respectively. The films in Fig. 10(a) and
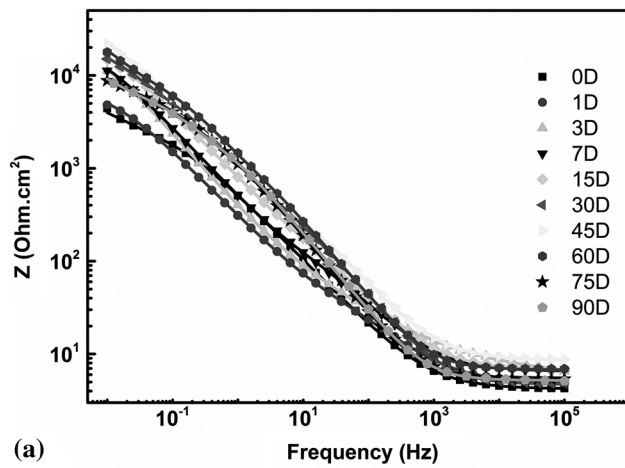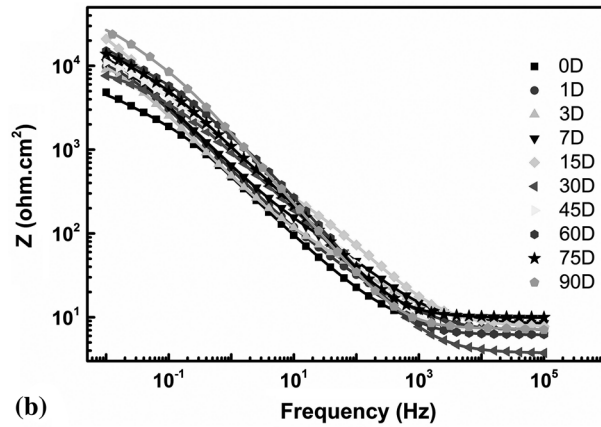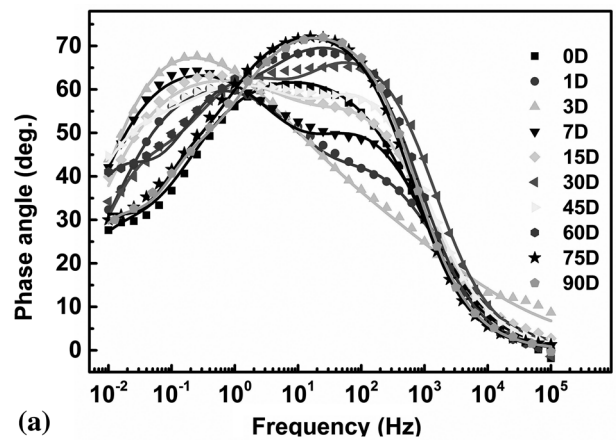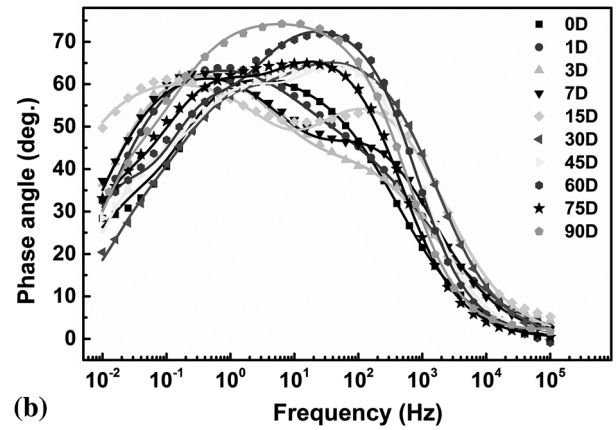
Fig. 5 Bode plots of Samples A, B and C after 0-, 1-, 3-, 7-, 15-, 30-, 45-, 60-, 75-, 90-day immersion in 3.5% NaCl solution

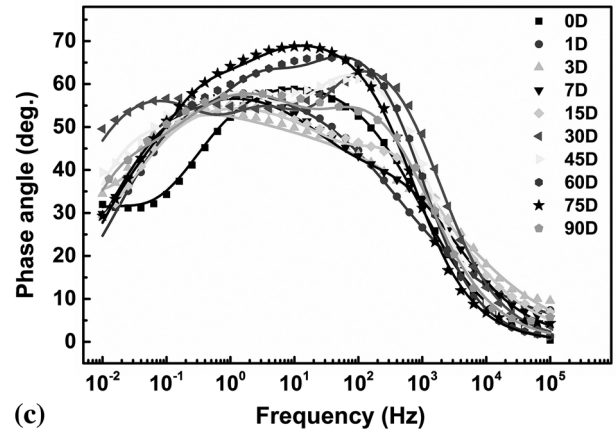**Fig. 6** Phase angle plots of Samples A, B and C after 0-, 1-, 3-, 7-, 15-, 30-, 45-, 60-, 75-, 90-day immersion in 3.5% NaCl solution

(b), approximately 2 μm in thickness, are slightly thinner than the film in Fig. 10(c). In Fig. 10(c), the film seems to be divided into two layers with the outer dark gray porous layer being thinner than the inner compact light gray layer. The films grew thicker as the immersion time is increased as presented in Fig. 11(a), (b) and (c). There are also two layers of films, the outer light gray layer and the inner dark gray layer, for Samples A and B. This is in agreement with the electrochemical result which reveals one layer of film for Samples A and B, and two layers for Sample C after 15-day immersion, and two layers for all the three samples after 30-day immersion. This confirms that the films gradually grow in thickness with increasing resistance

as the immersion time is increased which is in line with previous reports (Ref 14, 21).

Micrographs of the corrosion product film on the three samples after 15 and 30 days are shown in Fig. 12 and 13, respectively. Figure 12(a) shows the surface film with agglomerates of triangle- or diamond-shaped particles. The alloy surface is not completely covered with the film particles, thereby exposing itself to chloride ions attack. Figure 12(b) shows particles slightly smaller than Fig. 12(c), although the morphology of both is similar. It can be inferred that the growth rate of the oxide film is in the order of Tube C > Tube B > Tube A after 15-day immersion.
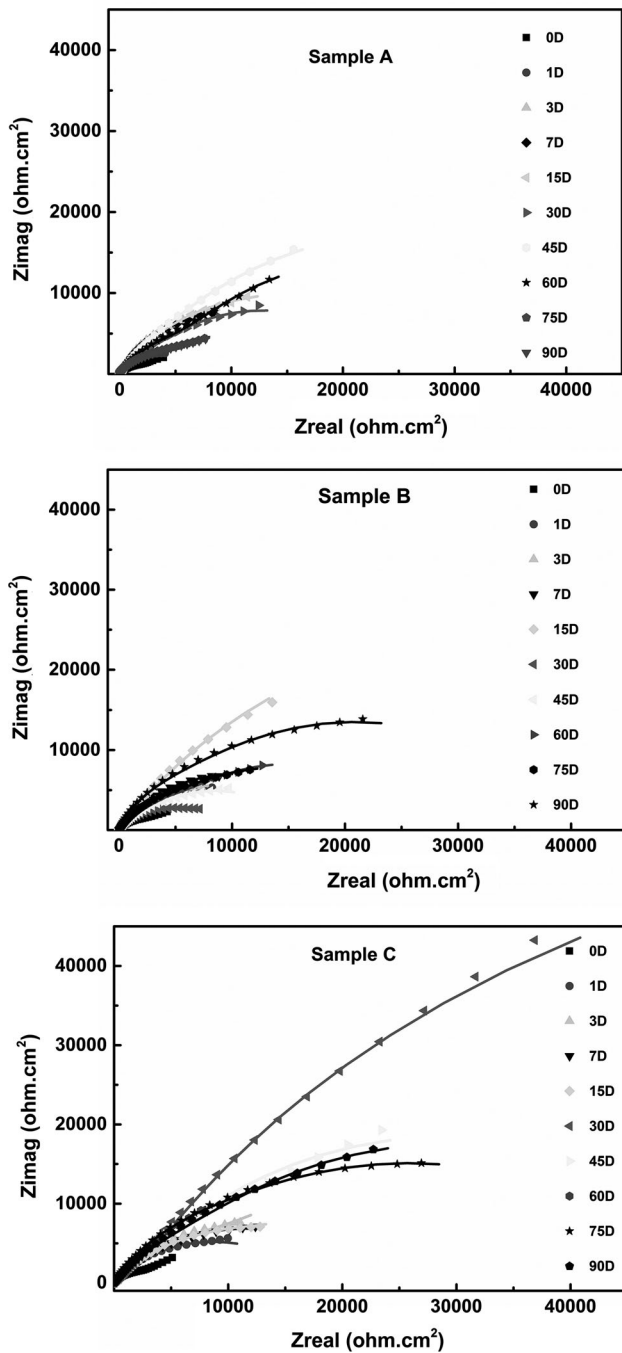
Fig. 7 Nyquist plots of Samples A, B and C after 0-, 1-, 3-, 7-, 15-, 30-, 45-, 60-, 75-, 90-day immersion in 3.5% NaCl solution

In Fig 13(a), it is found that the surface film on Sample A grows thicker with triangle- or diamond-shaped particles evenly distributed on the substrate. The corrosion resistance of the three tubes is dependent on the compact nature of the underlying inner film, R_{f2}, which is covered by the porous outer layer R_{f1} (Ref 10, 11, 16, 20, 32) as revealed by EIS result in Tables 6 and 7. But increasing porosity of the surface film will finally lead to loss of barrier properties of the inner layer as the inner or barrier layer will be attacked by high concentration of chloride ions penetrated through the outer layer from the solution after long time's interaction (Ref 31).

The XRD patterns for the corrosion product film formed on the surface of the three samples after 15- and 30-day immersion in simulated seawater are presented in Fig. 14 and 15, respectively. It is supposed that the Cu characteristic peaks in all the XRD patterns are from the alloy substrate. The peaks in Sample C (Fig. 14c) reveal the presence of paratacamite [$Cu_2(OH)_3Cl$] which has been reported by several authors (Ref 16, 33-35) to be present on the surface of Cu-Ni alloys. Ni-rich paratacamite (($Cu,Ni)_2(OH)_3Cl$) is observed to be present in the surface film of the three samples after 15-day immersion. It is therefore necessary to conclude that the corrosion product film of the samples is rich in nickel at the early days of immersion.

However, after 30-day immersion Fig. 15(a) (Sample A) reveals the presence of cupric oxide, CuO, on the film surface in addition to Ni-rich paratacamite, which indicates that changes in the nature of the film with time and $Cu_2(OH)_3Cl$ and $Cu(OH)_2 \cdot 2H_2O$ are detected on the surface film of Samples B and C after 30-day immersion period as shown in Fig. 15(b) and (c). CuO has been found to be the hydrolyzed product of cuprous oxide (Cu_2O) when immerse in seawater (Ref 34). Chauhan et al. (Ref 36) reported that on initial immersion of Cu-Ni alloys, Cu_2O is formed, but complex changes occur with continuous exposure (Ref 7). The passive film layer formed on the alloy surface is known to contain an outer CuO layer with chemisorbed water molecules and traces of chloride ions, and an inner Cu_2O layer containing Ni^{2+} and Ni^{3+} (Ref 23, 25, 32, 37) which may be converted to CuO, $Cu_2(OH)_3Cl$ (paratacamite), ($Cu,Ni)_2(OH)_3Cl$ (Ni-rich paratacamite) and $Cu(OH,Cl)_2 \cdot 2H_2O$ (calumetite) through hydrolysis and complex reaction with chloride ions from the solution. Since $Cu_2(OH)_3Cl$ has no significant effect on the corrosion resistance of the corrosion product film (Ref 38), $Cu_3(OH)_2Cl_4$ and $Cu(OH,Cl)_2 \cdot 2H_2O$ detected after 30 days can be assumed to be non-protective also, but the presence of Ni in the corrosion product has been speculated to increase resistance to corrosion. We can therefore suggest that the Ni-rich paratacamite may have improved the corrosion resistance of the three samples during the early days of immersion.

3.7 Depth Profile Analysis Using XPS

Depth profiles of main elements after 15-day immersion for the outer layer within the sputtering range of 0-1260 s at the original film surface and the inner layer within the sputtering range of 0-300 s at the slope between the exposed alloy substrate and the original film surface formed by the scrapping process are presented in Fig. 16 for Samples A, B and C, respectively. Existence of Ni in the outer layer of the corrosion product film is illustrated in Fig. 16(a), (b) and (c) which is in good agreement with XRD results (Fig. 14). Figure 16(a′), (b′) and (c′) shows extreme enrichment of Ni content in the inner layer indicating increase in Ni from the outer surface to the inner layer.

Figure 17(a), (b) and (c) presents spectra of Ni $2p$ corresponding to the outer layer in the sputtering range of 140-1260 s of the corrosion product film for Samples A, B and C after 15-day immersion, while Fig. 18(a), (b) and (c) shows the counterparts of the inner layer in the sputtering range of 60-300 s. During fitting, the double nature of Ni $2p$ lines was taken into consideration and the lines were fitted with peak pairs with similar intensity ratio, width and binding energy separation of ~6 eV (Ref 39). High enrichment of Ni

Table 5 Circuit parameters fitted from the EIS result for Sample A after immersion in 3.5 wt.% NaCl solution

Time, days	R_s, Ω cm²	Y_1, Ω s^{-1} cm² s^n	n_1	R_{ct}, Ω cm²	Y_2, Ω s^{-1} cm^{-2} s^n	n_2	R_{f1}, Ω cm²	Y_3, Ω s^{-1} cm^{-2} s^n	n_3	R_{f2}, Ω cm²	R_{Total}, Ω cm²	χ^2
0	4.20	0.0006	0.738	1770	0.0020	0.69	5930	...	...	...	7700	5E−04
1	4.82	0.0010	0.652	23	0.0009	0.73	8050	...	...	...	8073	3E−04
3	5.67	0.0032	0.410	148	0.0006	0.83	20,300	...	...	...	20,448	6E−04
7	6.50	0.0006	0.700	64	0.0005	0.76	24,500	...	...	...	24,564	4E−04
15	6.77	0.0007	0.741	38	0.0003	0.73	30,400	...	...	...	30,438	4E−04
30	4.75	0.0003	0.972	13	0.0001	0.83	316	0.0001	0.466	40,700	41,029	2E−04
45	8.61	0.0006	0.736	1970	0.0003	0.85	55	0.0003	0.751	53,300	55,325	3E−04
60	6.87	0.0003	0.940	18	0.0001	0.86	1392	0.0002	0.424	182,000	183,410	2E−04
75	5.36	0.0003	0.847	1060	0.0004	0.86	4270	0.0017	0.815	16,100	21,430	3E−04
90	5.18	0.0004	0.871	3850	0.0003	0.84	1020	0.0018	0.885	10,300	15,170	2E−04

Table 6 Circuit parameters fitted from the EIS result for Sample B after immersion in 3.5 wt.% NaCl solution

Time, days	R_s, Ω cm²	Y_1, Ω s^{-1} cm^{-2} s^n	n_1	R_{ct}, Ω cm²	Y_2, Ω s^{-1} cm^{-2} s^n	n_2	R_{f1}, Ω cm²	Y_3, Ω s^{-1} cm^{-2} s^n	n_3	R_{f2}, Ω cm²	R_{Total}, Ω cm²	χ^2
0	6.72	0.0010	0.65	6940.0	0.0011	0.87	847	...	...	...	7787	5E−04
1	6.28	0.0019	0.54	33.2	0.0004	0.76	15,300	...	...	...	15,333	2E−04
3	7.94	0.0009	0.59	61.2	0.0005	0.76	16,200	...	...	...	16,261	5E−04
7	8.36	0.0004	0.68	61.8	0.0004	0.75	21,200	...	...	...	21,262	5E−04
15	7.71	0.0002	0.75	134.0	0.0003	0.71	86,800	...	...	...	86,934	6E−04
30	3.72	0.0004	0.77	2620.0	0.0007	0.82	84	0.0008	0.78	6780	9484	2E−04
45	6.60	0.0003	0.86	93.4	0.0003	0.81	2040	0.0005	0.79	13,300	15,433	6E−04
60	6.16	0.0002	0.87	542.0	0.0003	0.87	5160	0.0007	0.85	19,700	25,402	5E−04
75	9.88	0.0003	0.81	4870.0	0.0006	0.80	19,900	0.0005	0.83	154	24,924	3E−04
90	6.62	0.0000	0.81	0.7	0.0003	0.85	31,800	0.0002	0.85	6450	38,251	4E−04

Table 7 Circuit parameters fitted from the EIS result for Sample C after immersion in 3.5 wt.% NaCl solution

Time, days	R_s, Ω cm²	Y_1, Ω s^{-1} cm^{-2} s^n	n_1	R_{ct}, Ω cm²	Y_2, Ω s^{-1} cm^{-2} s^n	n_2	R_{f1}, Ω cm²	Y_3, Ω s^{-1} cm^{-2} s^n	n_3	R_{f2}, Ω cm²	R_{Total}, Ω cm²	χ^2
0	3.85	0.0004	0.73	1140	0.0013	0.64	7910	...	...	...	9050	2E−04
1	5.05	0.0003	0.69	8480	0.0104	0.26	720,000	...	...	...	728,480	3E−04
3	6.60	0.0006	0.85	2640	0.0004	0.52	106,000	...	...	...	108,640	7E−04
7	6.38	0.0004	0.64	19	0.0003	0.68	11,600	...	...	...	11,619	2E−04
15	6.37	0.0001	0.92	11	0.0007	0.52	29,400	0.0006	0.71	6600	36,011	3E−04
30	8.79	0.0003	0.82	818	0.0001	0.92	129	0.0002	0.73	87,000	87,947	8E−04
45	6.37	0.0001	0.85	112	0.0002	0.78	1870	0.0004	0.78	26,200	28,182	8E−04
60	6.33	0.0001	0.84	1110	0.0002	0.86	67	0.0003	0.84	17,800	18,977	4E−04
75	6.58	0.0003	0.84	233	0.0002	0.84	3790	0.0004	0.78	19,900	23,923	5E−04
90	9.53	0.0001	0.81	53	0.0002	0.70	3870	0.0005	0.79	23,600	27,523	8E−04

in the inner layer (Fig. 18a-c) makes peak fitting and deconvolution much more reliable. The deconvolution of Ni 2p spectra of the outer film layer after sputtering for 140 s reveals three peaks for Sample A (Fig. 17a), centered at binding energies (B.E) of ∼853.9 eV assigned to NiO, ∼856.3 eV assigned to Ni(OH)$_2$ and ∼856.8 eV assigned to N$_2$O$_3$ with their shake up peaks centered at B.E ∼860, ∼861.1 and ∼863.2 eV, respectively. Similar compounds were detected for Samples B and C after the same sputtering time (140 s). After sputtering for 1260 s, strong peaks were observed indicating increase in the Ni content with sputtering time. Three peaks assigned as NiO, Ni(OH)$_2$ and N$_2$O$_3$ were deconvoluted for Sample A with B.E centered at ∼854.0, 856.1 and 856.8 eV, respectively. Two peaks were deconvoluted for Sample B with their B.E centered at 854.2 and 856.6 eV assigned as NiO and Ni$_2$O$_3$. Similarly, two peaks are deconvoluted for Sample C centered at the B.E of ∼854.3 and 856.6 eV for NiO and Ni$_2$O$_3$, respectively.

In the inner layer within the sputtering range of 60 and 300 s, very strong Ni 2p spectra are observed for the three samples as illustrated in Fig. 18, indicating increment in the Ni content from the outer layer to the inner one. The deconvolution of spectra from Samples A and C reveals only one peak centered at B.E of ∼852.3 eV assigned as metallic Ni. On the contrary for Sample B, in addition to metallic Ni peak, N$_2$O$_3$ peak is also observed.

Figure 19(a), (b) and (c) demonstrates depletion of Ni content on the surface of the corrosion product film as immersion time is increased to 30 days. This is in good agreement with the XRD results in Fig. 15. As shown in

Fig. 19(a′), (b′) and (c′), the inner layer remained rich in Ni as the immersion time is increased.

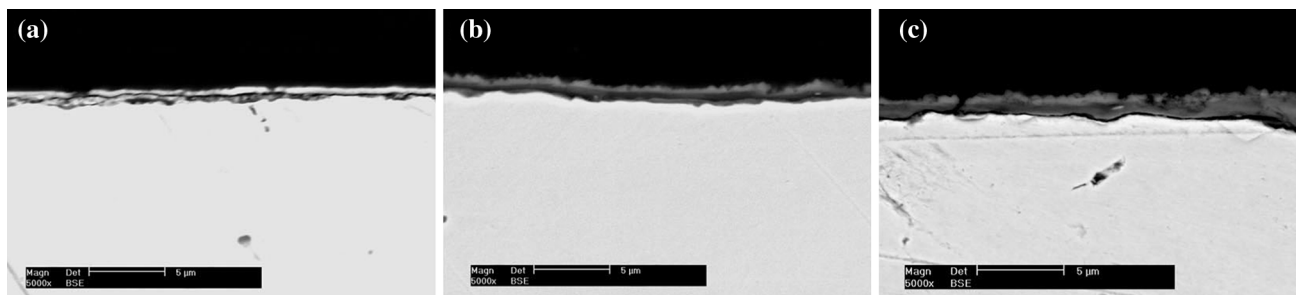Figure 20(a), (b) and (c) depicts the Ni 2p spectra of the samples after 30-day immersion in 3.5% NaCl solution for the outer layer after 140 and 1260 s sputtering time for Samples A, B and C, respectively. It can be seen that after sputtering for 140 s, the Ni 2p spectra of the samples were so weak to the extent that fitting was not possible. However, at sputtering time of 1260 s, the deconvolution gave rise to a peak centered at B.E
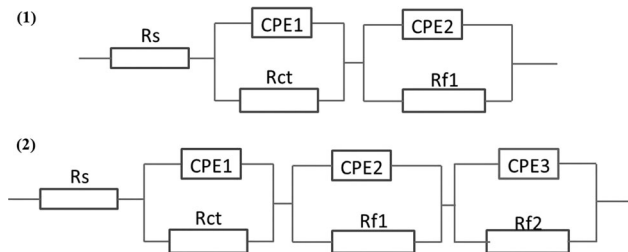
Fig. 8 Equivalent circuits used for fitting the impedance spectra of the three alloy specimens after 0-, 1-, 3-, 7-, 15-, 30-, 45-, 60-, 75-, 90-day immersion in 3.5% NaCl solution. Circuit 1 fit Samples A and B till after 15-day immersion time and Sample C to 7-day immersion time. Circuit 2 was used to fit Samples A and B from 30- to 90-day immersion period, while it fit Sample C from 15- to 90-day immersion period
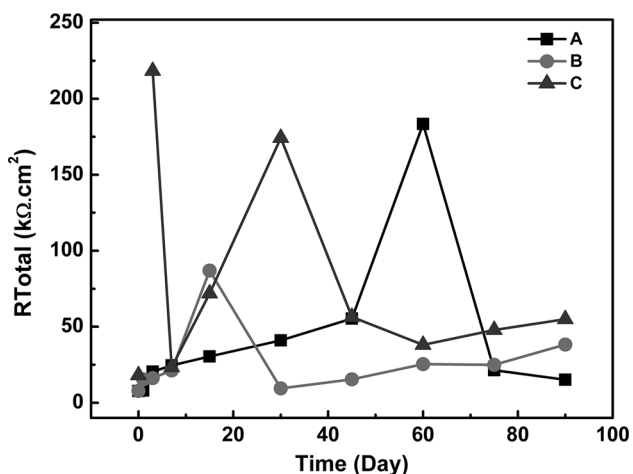
Fig. 9 Comparison of the resultant resistance of the films, R_{Total} for the three samples after 0-, 1-, 3-, 7-, 15-, 30-, 45-, 60-, 75-, 90-day immersion in 3.5% NaCl solution

of ∼855.8 eV assigned as $Ni(OH)_2$ for Sample A and two peaks centered at B.E of ∼854.0 and 856.2 eV attributed to NiO and $Ni(OH)_2$, respectively, for Sample C, while the spectrum of Sample B remains weak. The presence of $Ni(OH)_2$ may be due to exposure in air before sample analysis.

The inner layer of the corrosion product produces Ni 2p spectra with high intensity as shown in Fig. 21. The deconvolution of Ni 2p spectra for Sample A (Fig. 21a) after sputtering for 60 and 300 s showed a single peak attributed to metallic Ni centered at B.E of ∼852.4 eV with its shake up peak at B.E of 858.3 eV. At the same sputtering range, the deconvolution of Ni 2p spectra for Sample B (Fig. 21b) resulted in two peaks centered at B.E of ∼852.3 and ∼855.4 eV assigned to metallic Ni and NiO with their shake up at B.E of ∼858.4 and 861.3 eV, respectively. The Ni 2p spectra for Sample C showed slightly different behavior after deconvolution as an oxidized specie of Ni is observed at higher sputtering time (300 s) and not at lower sputtering time (60 s) as shown in Fig. 21(c).

Ni in copper-nickel alloys has been widely reported by many authors to improve the corrosion resistance of the alloys in seawater (Ref 34, 35, 40). Ni from the alloy segregates into Cu_2O barrier layer via a solid-state reaction and Ni^{2+} interacts with mobile cation vacancy which leads to a decreased ionic conductivity, thereby increasing electronic conductivity of the barrier film and the corrosion resistance is thus increased (Ref 38, 41). In this present study, XRD (Fig. 14, 15) and XPS (Fig. 16, 19) analyses revealed enrichment of Ni in the corrosion product film of the three samples. As shown in Fig. 14, the outer surface of the three samples is rich in Ni with its incorporation into $Cu_2(OH)_3Cl$ to form $(Cu,Ni)_2(OH)_2Cl$ by substituting Cu^{2+}. The corrosion rate of Ni is known to be at least two orders of magnitude lower than Cu (Ref 39). Therefore, the corrosion product film of the samples is enriched in metallic Ni during the early stages of the immersion (15 days) in 3.5 wt.% NaCl solution due to the corrosion rate of Ni being significantly lower than Cu. It can be suggested that the corrosion resistance of these alloys in simulated seawater is greatly influenced by Ni enrichment of the corrosion product film formed on the samples. While the outer surface is enriched with Ni at the early immersion, maximum enrichment is reached at the inner layer. The extent of enrichment varies from sample to sample as demonstrated by XPS result in Fig. 16 and 19.

The presence of NiO, Ni_2O_3 and $Ni(OH)_2$ in corrosion product film has been speculated to be through oxidation of metallic Ni (Ref 40). NiO is thermodynamically more stable than Cu_2O. Therefore, the presence of NiO in the corrosion product film gives it more stability and improves
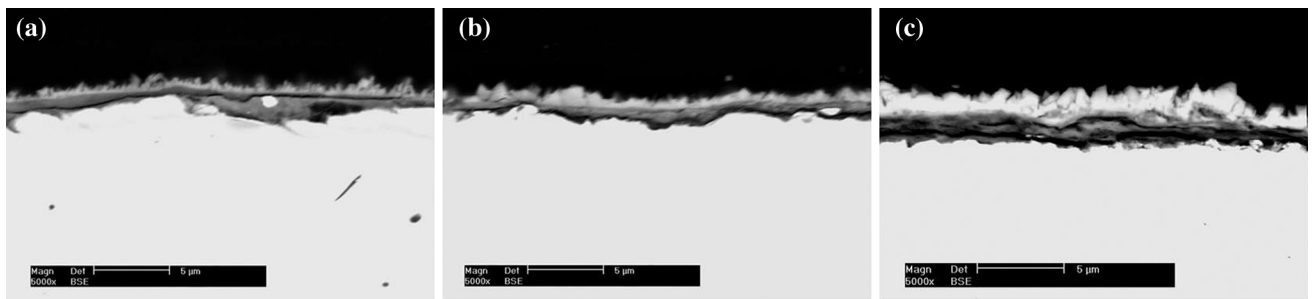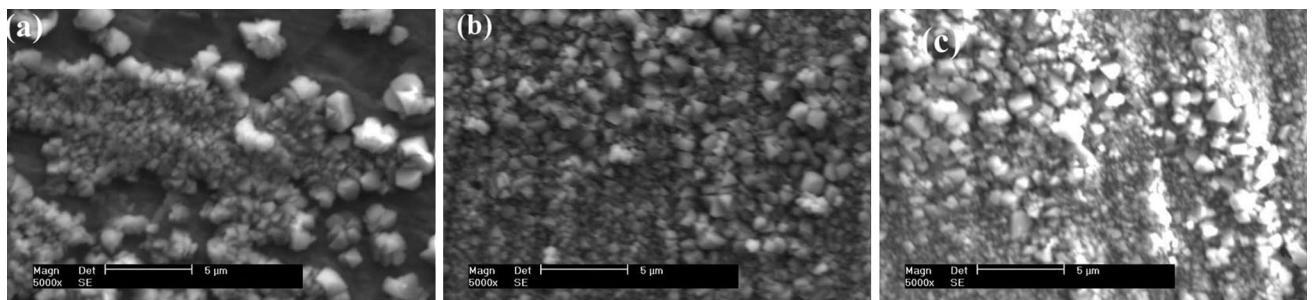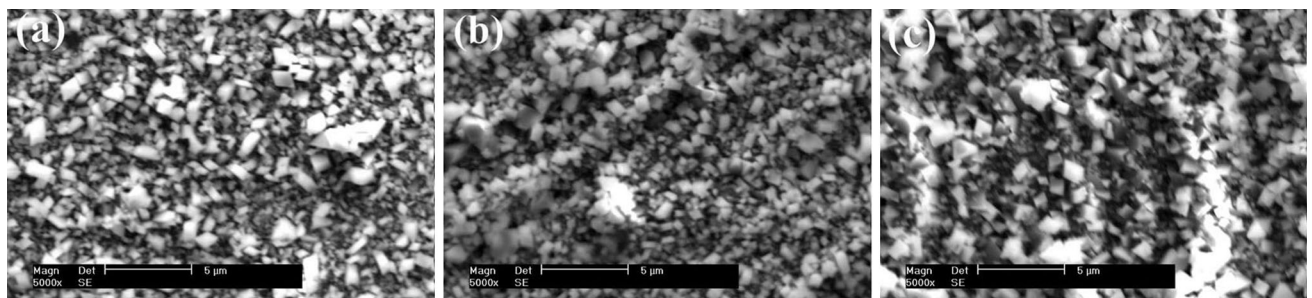

Fig. 10 SEM cross-sectional morphology of the corrosion product film formed on Tubes A, B and C (a, b and c), respectively, after 15-day immersion in 3.5% NaCl solution
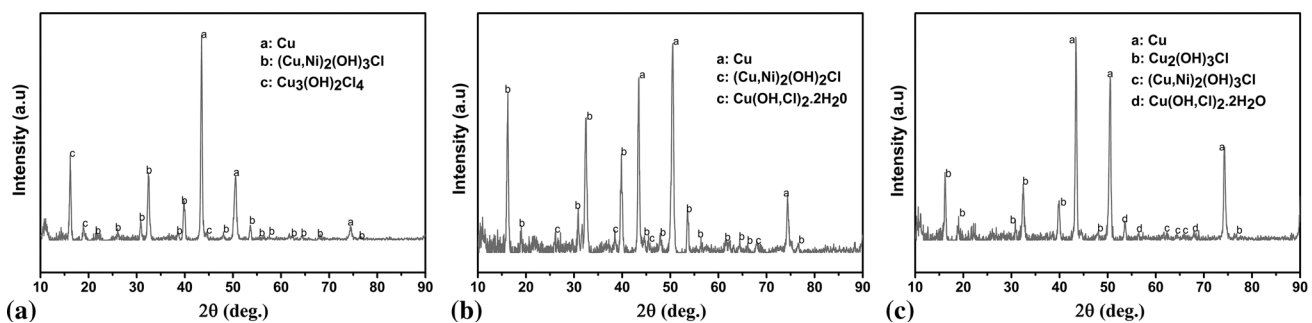
Fig. 11 SEM cross-sectional morphology of the corrosion product film formed on Tubes A, B and C (a, b and c), respectively, after 30-day immersion in 3.5% NaCl solution

Fig. 12 SEM surface morphology of the corrosion product film formed on Tubes A, B and C (a, b and c), respectively, after 15-day immersion in 3.5% NaCl solution
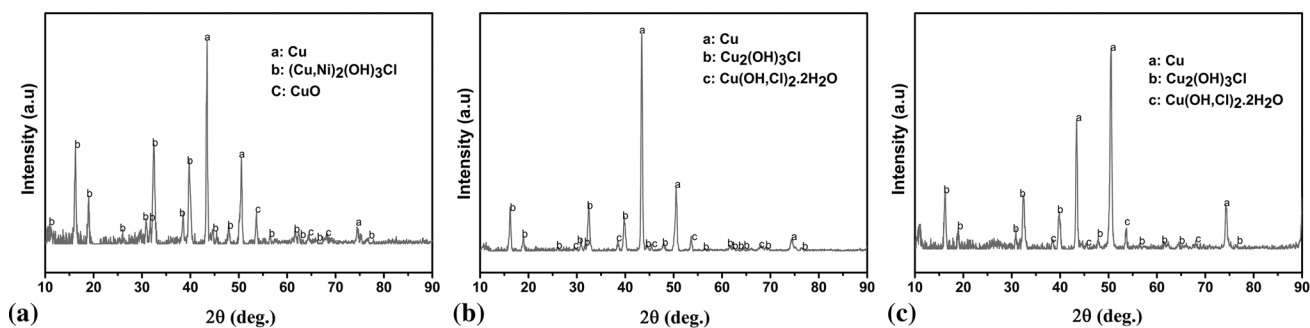

Fig. 13 SEM surface morphology of the corrosion product film formed on Tubes A, B and C (a, b and c), respectively, after 30-day immersion in 3.5% NaCl solution

Fig. 14 The XRD patterns of the corrosion product formed on the surface of Tubes A, B and C (a, b and c), respectively, after 15-day immersion in 3.5% NaCl solution

corrosion resistance of the film (Ref 38, 41). It can be concluded that the good corrosion behavior of Sample C after 30 days is due to the presence of NiO into its inner film layer.

3.8 Oxidation and Formation Process of Cu$_2$O Film

Copper-nickel alloy forms a layer of oxide film when immersed in seawater. The properties such as chemical nature

Fig. 15 The XRD patterns of the corrosion product formed on the surface of Tubes A, B and C (a, b and c), respectively, after 30-day immersion in 3.5% NaCl solution
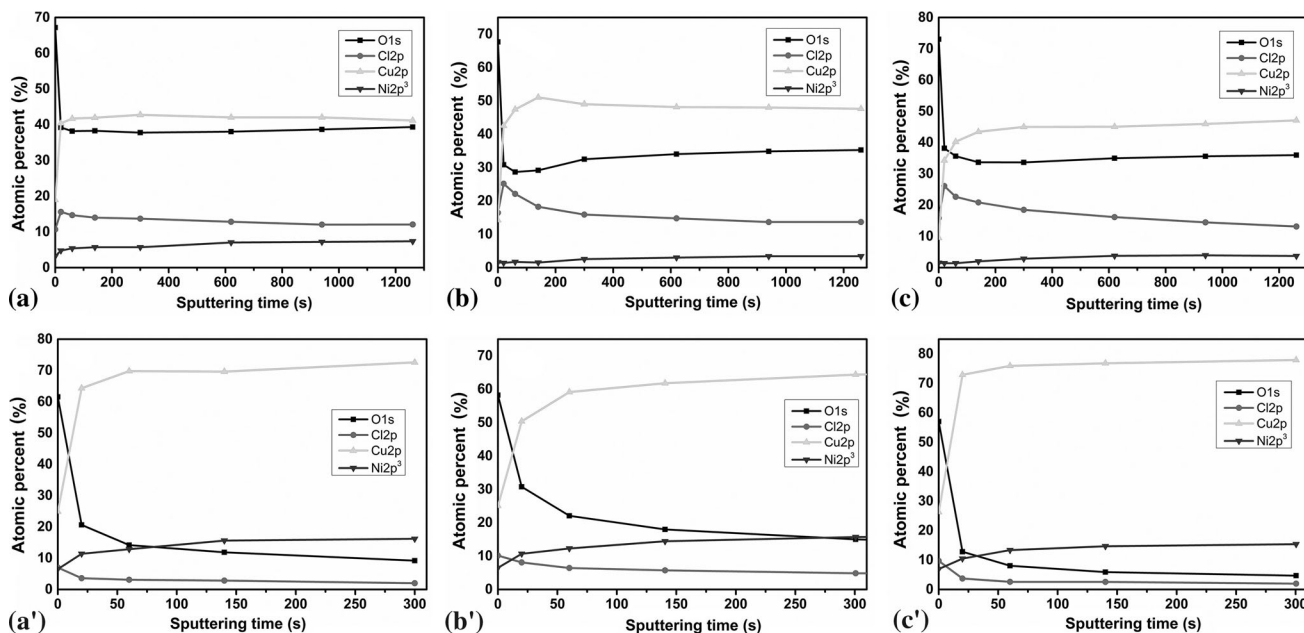

Fig. 16 Depth profiles of elements sputtered at the original surface (a, b and c) and at the slope (a′, b′, c′) between the exposed alloy substrate and the original surface formed by the scrapping process to the corrosion product film on Samples A (a, a′), B (b, b′) and C (c, c′), respectively, after 15-day immersion in 3.5% NaCl solution

and the thickness of the oxide film have significant effect on the corrosion resistance of the copper-nickel alloy in seawater. Kear et al. (Ref 41) reported that rapid increase in current densities at the anodic region is due to the formation of a soluble $CuCl_2^-$ and other soluble species such as:

$$Cu + 2Cl^- \rightarrow CuCl_2^- + e^- \qquad (Eq\ 2)$$

$$CuOH^-ads + OH^- \rightarrow Cu(OH)_2^- aq + e^- \qquad (Eq\ 3)$$
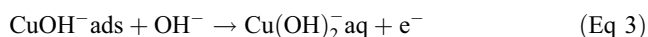
This process exposes the metal surface to further attack leading to a decrease in the OCP as immersion time is increased. It has been suggested that the presence of high concentration of $CuCl_2^-$ at the metal surface leads to hydrolysis reaction and formation of Cu_2O (Ref 42) which is passive and protective.

$$2CuCl_2^- + H_2O \rightarrow Cu_2O + 4Cl^- + 2H^+. \qquad (Eq\ 4)$$
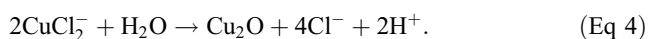
The evolution of Cu_2O layer, known to be protective, causes the transition from active to passive behavior, thereby shifting the OCP of the three samples to more positive values. This is indicated by a decrease in the corrosion current densities of the

working electrode as shown by potentiodynamic polarization data in Tables 2 and 3. This is in good agreement with what has been proposed previously by other researchers (Ref 31). Linear polarization resistance as well as EIS also revealed increase in the corrosion resistance with time which is due to the formation of protective oxide film on the surface of the metals.

Cu_2O in Eq 4 is thermodynamically unstable, and it can therefore be oxidized into cupric ions (Ref 6, 43). As the immersion time is increased, the Cu_2O film thickens; meanwhile, oxidation transformation of the Cu_2O at the surface of the film to cupric oxide (CuO) or cupric hydroxide ($Cu(OH)_2$) probably occurs (Ref 43) as shown in the equations below:

$$Cu_2O + H_2O \rightarrow 2CuO + 2e^- + 2H^+ \qquad (Eq\ 5)$$

$$Cu_2O + 3H_2O \rightarrow 2Cu(OH)_2 + 2e^- + 2H^+ \qquad (Eq\ 6)$$
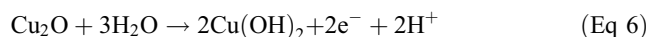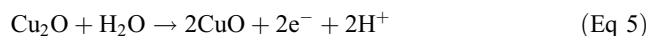
This is in agreement with the XRD results especially for Sample A (Fig. 15a) which reveals the presence of CuO on the surface film.

The formation of the oxide and hydroxide in Eq 5 and 6 which are not protective led to loss of barrier properties, and this
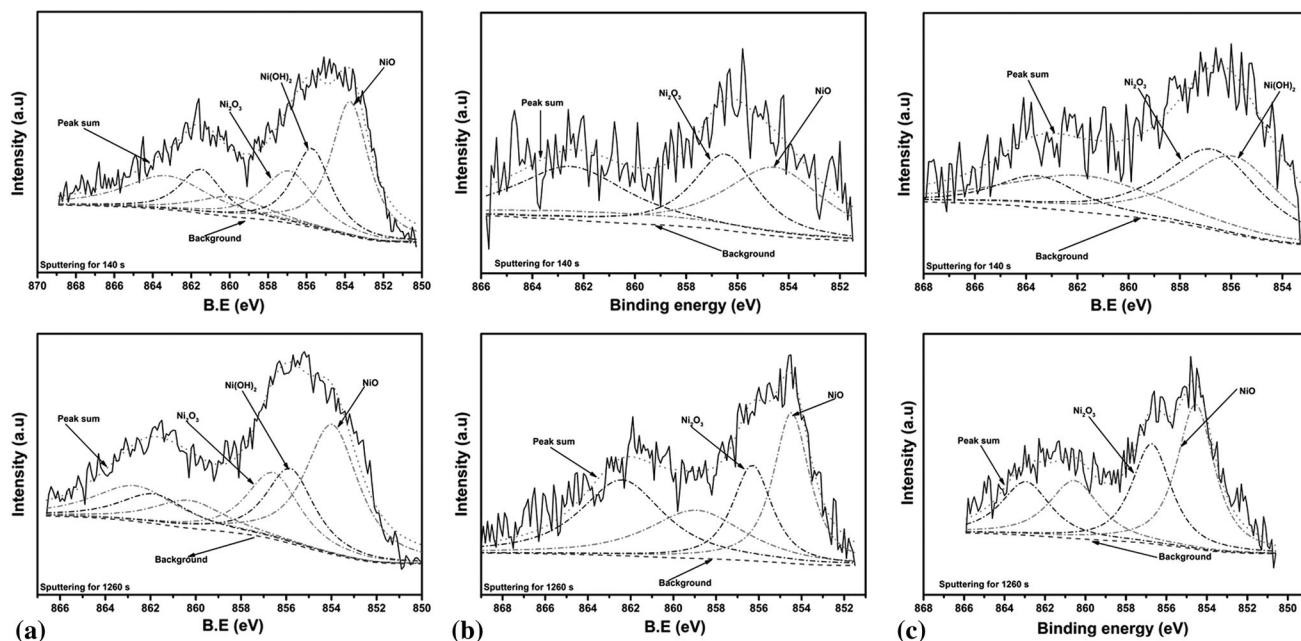
Fig. 17 XPS spectra of Ni 2p of the original surface of corrosion product film sputtered for 140 and 1260 s on Samples A (a), B (b) and C (c) after 15-day immersion in 3.5% NaCl solution
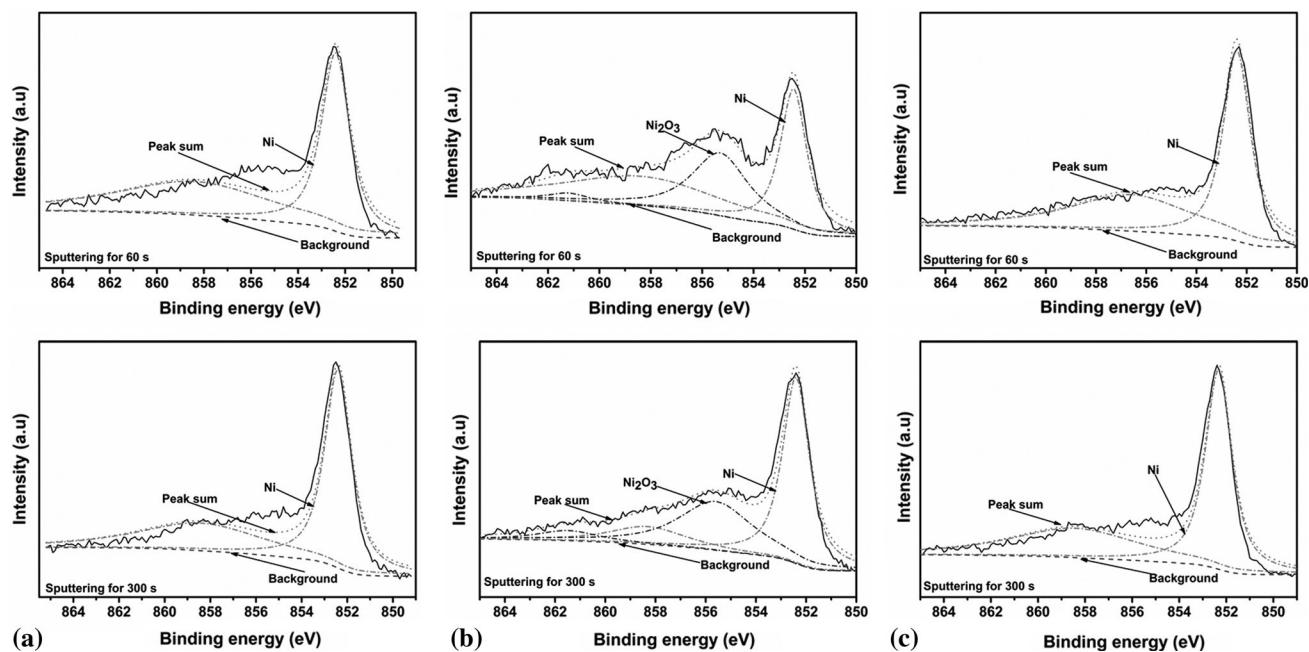
Fig. 18 XPS spectra of Ni 2p sputtered for 20 and 300 s at the slope between the exposed alloy substrate and the original surface after scrapping process to the corrosion product film on the Samples A (a), B (b) and C (c) after 15-day immersion in 3.5% NaCl solution

resulted in a decrease in the film resistance as shown by outer film resistance beyond 30-day immersion. It has been reported that loss of barrier properties is attributed to the penetration of the electrolyte through the pores of the film (Ref 14). It therefore means that the porosity of the outer layer will expose the inner barrier layer to the attack of Cl$^-$ after long immersion time.

The inner layer of the corrosion product films is rich in Ni which exists in oxidized forms as NiO/Ni$_2$O$_3$ and metallic form as demonstrated by XPS analysis (Fig. 16, 17, 18, 19, 20, 21). The presence of NiO/Ni$_2$O$_3$ in the inner layer of corrosion product improves the corrosion resistance of the inner layer at longer immersion period as illustrated by EIS results in Tables 5, 6, and 7. Small amount of Ni were detected on the surface of the corrosion product film after 15 days, and this contributed to the stability and higher resistance of the film at early immersion.

4. Conclusion

1. OCPs of the three samples showed similar behavior as they initially shifted to more negative potentials with increase in
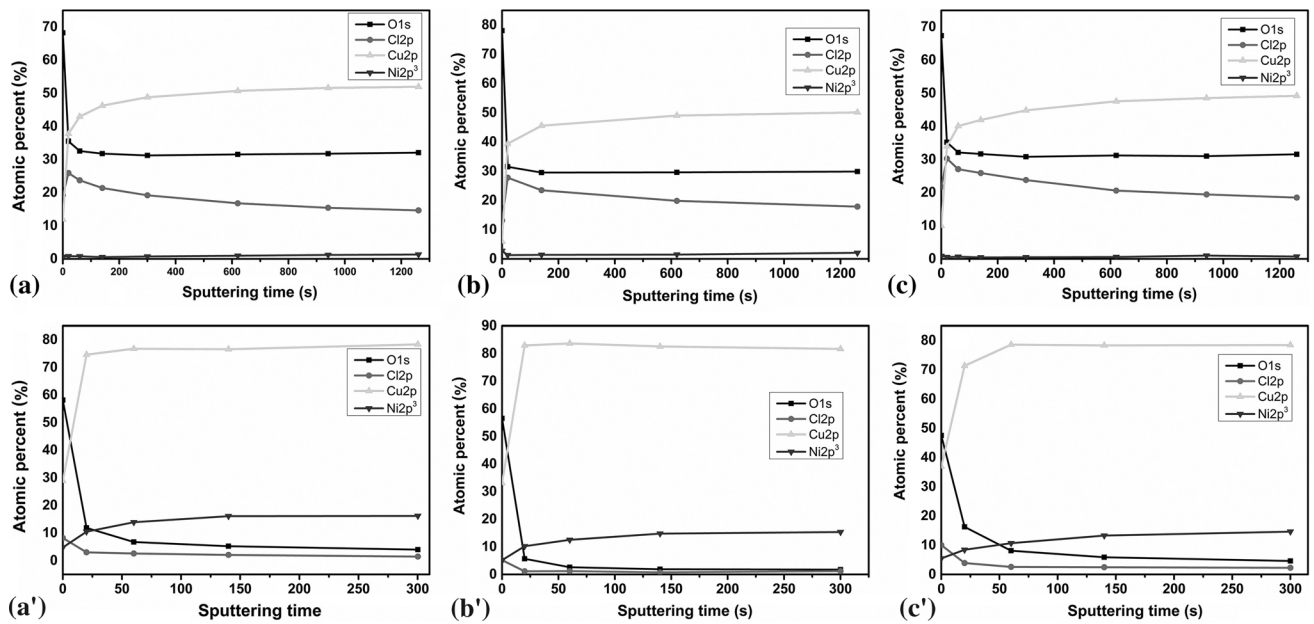
Fig. 19 Depth profiles of elements sputtered at the original surface (a, b and c) and at the slope (a′, b′, c′) between the exposed alloy substrate and the original surface formed by the scrapping process to the corrosion product film on Samples A (a, a′), B (b, b′) and C (c, c′), respectively, after 30-day immersion in 3.5% NaCl solution
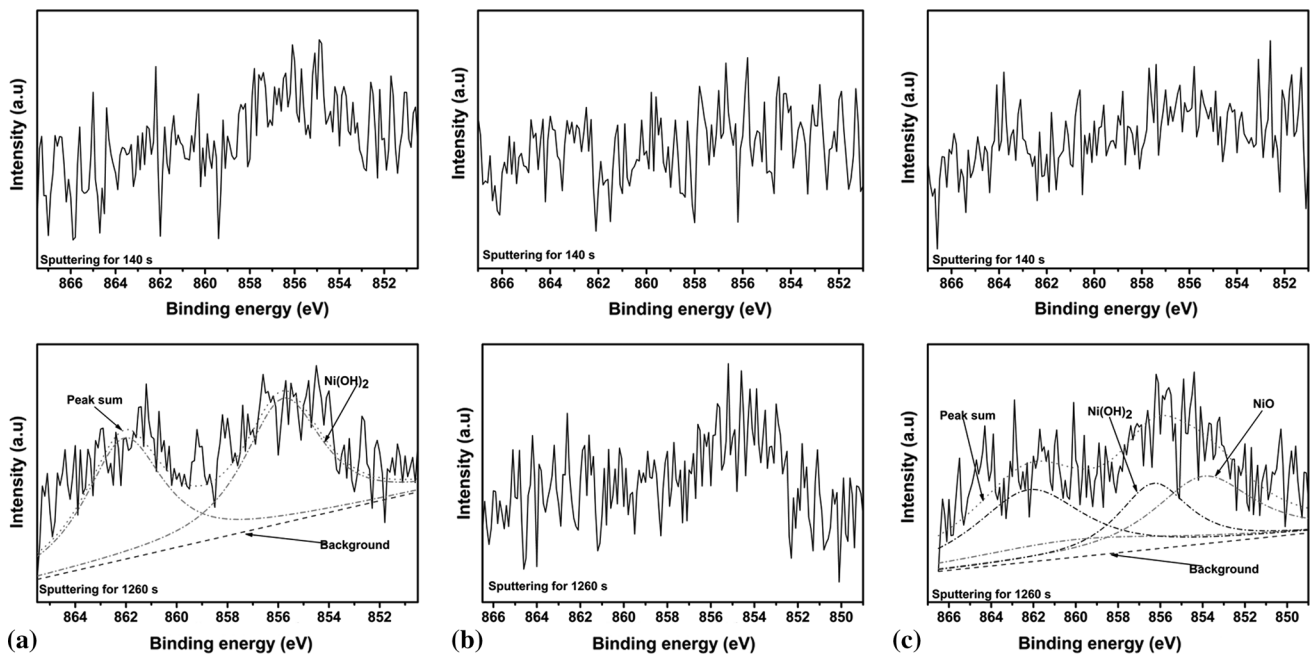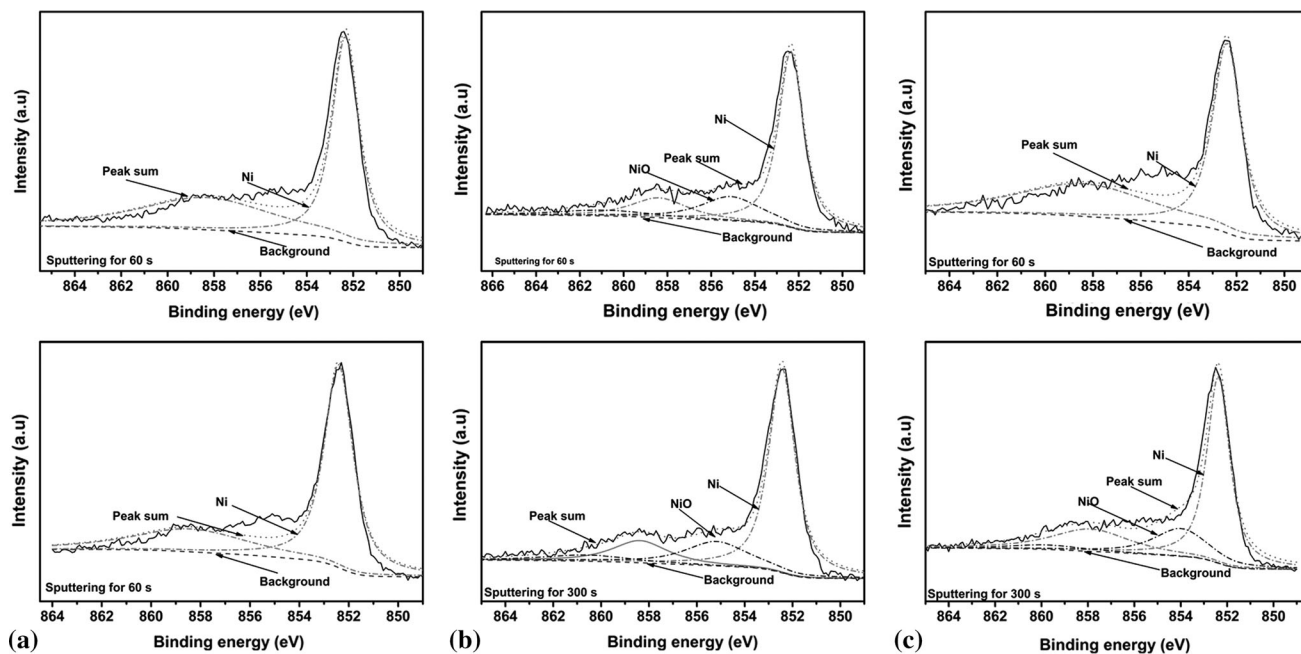

Fig. 20 XPS spectra of Ni 2p of the original surface of corrosion product film sputtered for 140 and 1260 s on Samples A (a), B (b) and C (c) after 30-day immersion in 3.5% NaCl solution

the immersion time before shifting to more positive values at longer immersion periods. However, the three samples showed active-passive transition at different times.

2. Formation of the inner compact oxide film layer did not take place at the same time for the three samples as it was revealed for Sample C earlier than Samples A and B. The better corrosion behavior of Sample C is due to early formation of the duplex layer of the protective oxide film in addition to very high film resistance at early immersion time which helps the sample to maintain good

resistance to corrosion throughout the immersion period.

3. The surface films of the three samples are rich in Ni at the early immersion stage, but depletion occurs at longer immersion, while it remains considerably constant in the inner film. Ni enriched in the outer layers exists in the form of Ni^{2+} and Ni^{3+} and is incorporated into $Cu_2(OH)_3Cl$ to form $(Cu,Ni)_2(OH)_3Cl$.

4. The corrosion product films of the three samples after immersion in simulated seawater are poor in Fe both at early and longer immersion period.

Fig. 21 XPS spectra of Ni 2*p* sputtered for 20 and 300 s at the slope between the exposed alloy substrate and the original surface after scrapping process to the corrosion product film on the Samples A (a), B (b) and C (c) after 30-day immersion in 3.5% NaCl solution

References

1. N. Acuña, B. Valdez, M. Schorr, and G. Hernández-Duque, Effect of Marine Biofilm on Fatigue Resistance of Austenitic & Stainless Steel, *Corros. Rev.*, 2004, **22**(2), p 101–113

2. R.W. Cahn, P. Hassen, and E.J. Kramer, Materials Science and Technology, A Comprehensive Treatment, *Structure and Properties of Nonferrous Alloys*, VCH, New York, 1996

3. J.M. Popplewell, R.J. Hart, and J.A. Ford, The Effect of Iron on the Corrosion Characteristics of 90-10 Cupronickel in Quiescent 3.4%NaCl Solution, *Corros. Sci.*, 1973, **13**, p 295–309

4. W.C. Stewart and F.L. Laque, Corrosion Resisting Characteristics of Iron Modified 90:10 Cupronickel Alloy, *Corrosion*, 1952, **8**, p 259–277

5. A.M. Beccaria and J. Crousier, Influence of Iron Addition on Corrosion Layer Built up on 70Cu-30Ni Alloy in Seawater, *Br. Corros. J.*, 1991, **26**, p 5

6. S.A. Campbell, G.J.W. Radford, C.D.S. Tuck, and B.D. Barker, Corrosion and Galvanic Compatibility Studies of a High-Strength Copper-Nickel Alloy, *Corrosion*, 2002, **58**(1), p 57–71

7. S. Colin, E. Beche, R. Berjoan, H. Jolibois, and A. Chambaudet, An XPS and AES Study of the Free Corrosion of Cu-, Ni- and Zn-Based Alloys in Synthetic Sweat, *Corros. Sci.*, 1999, **41**(6), p 1051–1065

8. G. Kear, B.D. Barker, K.R. Stokes, and F.C. Walsh, Electrochemistry of Non-Aged 90-10 Copper-Nickel Alloy (UNS C70610) as a Function of Fluid Flow: Part 2: Cyclic Voltammetry and Characterisation of the Corrosion Mechanism, *Electrochim. Acta*, 2007, **52**(7), p 2343–2351

9. R.C.N. Liberto, R. Magnabosco, and N. Alonso-Falleiros, Selective Corrosion of 550 °C Aged Cu10Ni-3Al-1.3Fe Alloy in NaCl Aqueous Solution, *Corros. Sci.*, 2011, **53**(5), p 1976–1982

10. R.F. North and M.J. Pryor, The Influence of Corrosion Product Structure on the Corrosion Rate of Cu-Ni Alloys, *Corros. Sci.*, 1970, **10**(5), p 297–311

11. P. Druska and H.H. Strehblow, Surface Analytical Examination of Passive Layers on Cu-Ni Alloys Part II. Acidic Solutions, *Corros. Sci.*, 1996, **38**(8), p 1369–1383

12. W. Schleich, *Typical Failures of CuNi 90/10 Seawater Tubing Systems and How to Avoid Them, European Corrosion Congress*, 2004, p 1–10

13. K.M. Wilhelm Schleich, and C. Powell, 5—CuNi 90/10: How to Avoid Typical Failures of Seawater Tubing Systems and Marine Biofouling on Structures, *Corrosion Behaviour and Protection of Copper and Aluminium Alloys in Seawater*, D. Féron, Ed., Woodhead Publishing, 2007, p 73–94

14. S.J. Yuan, A.M.F. Choong, and S.O. Pehkonen, The Influence of the Marine Aerobic Pseudomonas Strain on the Corrosion of 70/30 Cu-Ni Alloy, *Corros. Sci.*, 2007, **49**(12), p 4352–4385

15. R.J.K. Wood, S.P. Hutton, and D.J. Schiffrin, Mass Transfer Effects of Non-Cavitating Seawater on the Corrosion of Cu and 70Cu-30Ni, *Corros. Sci.*, 1990, **30**, p 1177–1201

16. A.L. Ma, S.L. Jiang, Y.G. Zheng, and W. Ke, Corrosion Product Film Formed on the 90/10 Copper-Nickel Tube in Natural Seawater: Composition/Structure and Formation Mechanism, *Corros. Sci.*, 2015, **91**, p 245–261

17. X.L. Zhu and T.Q. Lei, Characteristics and Formation of Corrosion Product Films of 70Cu-30Ni alloy in Seawater, *Corros. Sci.*, 2002, **44**(1), p 67–79

18. A. Ma, S. Jiang, Y. Zheng, Z. Yao, W. Ke, and S. Xia, Correlation Between Microstructure and Corrosion Behavior of Two 90Cu10Ni Alloy Tubes, *Acta Metall. Sin. (Engl. Lett.)*, 2014, **27**(4), p 730–738

19. W. Schleich, Application of Copper-Nickel Alloy UNS C70600 for Seawater Service, *CORROSION/2005 Annual Conference and Exhibition*, NACE International, Houston, 2005, p 1–14

20. M.S. Parvizi, A. Aladjem, and J.E. Castle, Behaviour of 90-10 Cupronickel in Sea Water, *Int. Mater. Rev.*, 1988, **33**(4), p 169–200

21. W.A. Badawy, M.M. El-Rabiee, N.H. Helal, and H. Nady, Effect of Nickel Content on the Electrochemical Behavior of Cu-Al-Ni Alloys in Chloride Free Neutral Solutions, *Electrochim. Acta*, 2010, **56**(2), p 913–918

22. A. Barbucci, G. Farne, P. Matteazzi, R. Riccieri, and G. Cerisola, Corrosion Behaviour of Nanocrystalline Cu90Ni10 Alloy in Neutral Solution Containing Chlorides, *Corros. Sci.*, 1998, **41**(3), p 463–475

23. W.A. Badawy, M. El-Rabiee, N.H. Helal, and H. Nady, The Role of Ni in the Surface Stability of Cu-Al-Ni Ternary Alloys in Sulfate-Chloride Solutions, *Electrochim. Acta*, 2012, **71**, p 50–57

24. F.M. Al-Kharafi and W.A. Badawy, Electrochemical Behaviour of Vanadium in aqueous Solutions of Different pH, *Electrochim. Acta*, 1997, **42**(4), p 579–586

25. K.M. Ismail and W.A. Badawy, Electrochemical and XPS Investigations of Cobalt in KOH Solutions, *J. Appl. Electrochem.*, 2001, **30**(11), p 1303

26. K.M. Ismail, A.M. Fathi, and W.A. Badaway, The Influence of Ni Content on the Stability of Copper-Nickel Alloys in Alkaline Sulphate Solutions, *J. Appl. Electrochem.*, 2004, **34**(8), p 823–831

27. I. Milošev and M. Metikoš-Huković, The Behaviour of Cu-xNi (x = 10 to 40 wt%) Alloys in Alkaline Solutions Containing Chloride Ions, *Electrochim. Acta*, 1997, **42**, p 1537–1548

28. R.G. Blundy and M.J. Pryor, The Potential Dependence of Reaction Product Composition on Copper-Nickel Alloys, *Corros. Sci.*, 1972, **12**, p 65–75

29. W.S. Tail, *An Introduction to Electrochemical Corrosion Testing for Practicing Engineers and Scientists*, University of Wisconsin-Madison, Racine, 1994

30. I. Thompson and D. Campbell, Interpreting Nyquist Responses from Defective Coatings on Steel Substrates, *Corros. Sci.*, 1994, **36**(1), p 187–198

31. A.M. Alfantazi, T.M. Ahmed, and D. Tromans, Corrosion Behavior of Copper Alloys in Chloride Media, *Mater. Des.*, 2009, **30**(7), p 2425–2430

32. K.M. Ismail, A.M. Fathi, and W.A. Badawy, Electrochemical Behavior of Copper-Nickel Alloys in Acidic Chloride Solutions, *Corros. Sci.*, 2006, **48**(8), p 1912–1925

33. L. Babouri, K. Belmokre, A. Abdelouas, J.F. Bardeau, and Y. El Mendili, The Inhibitive Effect of Cerium Carbonate on the Corrosion of Brass in 3% NaCl Solution, *Int. J. Electrochem. Sci*, 2015, **10**(9), p 7818–7839

34. K. Chandra, V. Kain, G.K. Dey, P.S. Shetty, and R. Kishan, Failure Analysis of Cupronickel Evaporator Tubes of a Chilling Plant, *Eng. Fail. Anal.*, 2010, **17**(2), p 587–593

35. B. Sun, T.Y. Ye, Q. Feng, J.H. Yao, and M. Wei, Accelerated Degradation Test and Predictive Failure Analysis of B10 Copper-Nickel Alloy under Marine Environmental Conditions, *Materials*, 2015, **8**(9), p 6029–6042

36. P.K. Chauhan and H.S. Gadiyar, An XPS Study of the Corrosion of Cu-10Ni Alloy in Unpolluted and Polluted Sea-Water: the Effect of $FeSO_4$ Addition, *Corros. Sci.*, 1985, **25**(1), p 55–68

37. J. Mathiyarasu, N. Palaniswamy, and V.S. Muralidharan, Effect of Nickel Content on the Electrochemical Behaviour of Cupronickel Alloy in Neutral Chloride Solutions, *Port. Electrochim. Acta*, 1999, **17**, p 45–56

38. M. Metikos-Hukovic, R. Babic, I. Skugor, and Z. Grubac, Copper-Nickel Alloys Modified with Thin Surface Films: Corrosion Behaviour in the Presence of Chloride Ions, *Corros. Sci.*, 2011, **53**(1), p 347–352

39. K.D. Efird, Potential-pH Diagrams for 90-10 and 70-30 Cu-Ni in Sea Water, *Corrosion*, 1975, **31**(3), p 77–83

40. Y.H. Kang, L.L. Luo, X. Tong, D. Starr, G. Zhou, and J.C. Yang, Duplex Oxide Formation During Transient Oxidation of Cu-5%Ni(001) Investigated by In Situ UHV-TEM and XPS, *8th International Symposium on High Temperature Corrosion and Protection of Materials (HTCPM), Les Embiez*, 2012

41. G. Kear, B.D. Barker, K. Stokes, and F.C. Walsh, Electrochemica Corrosion Behaviour of 90-10Cu-Ni Alloy in Chloride-Based Electrolytes, *J. Appl. Electrochem.*, 2004, **34**(7), p 659–669

42. C. Deslouis, B. Tribollet, G. Mengoli, and M.M. Musiani, Electrochemical Behaviour of Copper in Neutral Aerated Chloride Solution. II. Impedance Investigation, *J. Appl. Electrochem.*, 1988, **18**(3), p 384–393

43. R. Babic, M. Metikos-Hukovic, and M. Lonciar, Impedance and Photoelectrochemical Study of Surface Layers on Cu and Cu-10Ni in Acetate Solution Containing Benzotriazole, *Electrochim. Acta*, 1999, **44**(14), p 2413–2421